RADIAL WIDTHS, OPTICAL DEPTHS, AND ECCENTRICITIES OF THE URANIAN RINGS[a]

P. D. NICHOLSON[b]
Mount Stromlo and Siding Spring Observatories, Research School of Physical Sciences, Australian National University, Canberra, Australia

K. MATTHEWS
Downs Laboratory of Physics, 320-47, California Institute of Technology, Pasadena, California 91125

P. GOLDREICH
Division of Geological and Planetary Sciences, California Institute of Technology, Pasadena, California 91125

Received 15 June 1981; revised 5 October 1981

ABSTRACT

Observations of the stellar occultation by the Uranian rings of 15/16 August 1980 are used to estimate radial widths and normal optical depths for segments of rings 6, 5, 4, α, β, η, γ, and δ. Synthetic occultation profiles are generated to match the observed light curves. A review of published data confirms the existence of width-radius relations for rings α and β, and indicates that the optical depths of these two rings vary inversely with their radial widths. Masses are obtained for rings α and β, on the assumption that differential precession is prevented by their self-gravity. A quantitative comparison of seven ϵ-ring occultation profiles obtained over a period of 3.4 yr reveals a consistent structure, which may reflect the presence of unresolved gaps and subrings. Elliptical models for rings 6, 5, 4, α, β, and ϵ are presented for comparison with the results of previous studies, particularly that of Elliot *et al.* (1981a).

I. INTRODUCTION

Although observations of six stellar occultations by the rings of Uranus have been reported (Elliot *et al.* 1978 and references therein; Millis and Wasserman 1978; Nicholson *et al.* 1978; Hubbard and Zellner 1980; Nicholson, Matthews, and Goldreich 1981; Elliot *et al.* 1981a,b), several important questions concerning the structure of the rings remain unanswered. In particular, their intrinsic widths and optical depths are only poorly known, with the exception of the comparatively broad (20–100 km) ϵ ring. Several factors contribute to this state of affairs: the short duration of the ring occultations (typically 0.2–1.5 s, depending on the geocentric velocity of Uranus); broadening of the observed occultation profiles by diffraction, the finite angular diameter of the occulted star, and the instrumental response function; and noise in the recorded data.

By far the most favorable opportunity to improve our knowledge of the structure of the rings since their discovery in 1977 was provided by the stellar occultation of 15/16 August 1980—No. 12 in the list of Klemola and Marsden (1977). Not only is the star involved relatively bright ($K = 8.69$, Elliot *et al.* 1981a), but the geocentric velocity of Uranus was a rather low 8 km s^{-1}. Observations of the ring occultations on this date made at Las Campanas Observatory in Chile form the principal subject of this paper. The accompanying planetary occultation will be discussed elsewhere.

Observations of this event have also been reported by Bouchet, Perrier, and Sicardy (1980) and by Elliot *et al.* (1981a), working at ESO and CTIO, respectively. All three sets of data were obtained at a wavelength of 2.2 μm, and the maximum separation between the three telescopes (Las Campanas – CTIO) is 130 km. Elliot *et al.* (1981a) have combined the CTIO and ESO observations with published data from four earlier occultations in a new astrometric solution for the semimajor axes, eccentricities, and apsidal precession rates of the nine rings. This solution involved a determination of the orientation of the ring plane, previously assumed to coincide with the satellites' orbital plane as determined by Dunham (1971), which resulted in a systematic decrease of $\sim$90 km in the semimajor axes of all nine rings. Because the observations presented here provide essentially no new information on the geometry of the rings beyond that incorporated in the above solution, the emphasis of our analysis is on modeling the detailed structure of the ring occultation profiles. However, for the purpose of comparison with the results of Elliot *et al.*, we present in Sec. VI a set of independently derived elliptical models for rings 6, 5, 4, α, β, and ϵ.

II. OBSERVATIONS

The observations of 15/16 August 1980 were made on the 2.5-m du Pont telescope at Las Campanas, at an effective wavelength of 2.2 μm ($\Delta\lambda = 0.4$ μm). Instrumental setup and observational procedure were essentially the same as those adopted for two previous occul-

[a]Observations were made at Las Campanas Observatory as part of a joint agreement between the California Institute of Technology and the Carnegie Institution of Washington.

[b]Present address: Jet Propulsion Laboratory, 183-501, 4800 Oak Grove Drive, Pasadena, California 91109.

 0004-6256/82/020433-15$00.90

tations (Nicholson *et al.* 1978, 1981), and will not be described in detail here. The chopping frequency for sky subtraction was 35 Hz, and the chop amplitude 12 arcsec. The lock-in amplifier was operated with a 6 dB per octave rolloff 100-ms time constant, the data being recorded on a strip chart along with timing marks at intervals of 1 s synchronized with WWV. Measurements of the response of this recording system to a step function, generated by rapidly offsetting the chopper, yielded an overall system time constant of 100 ± 20 ms.

Observations commenced at 21:44 UTC on 15 August 1980, before sunset, and continued with minimal interruptions to 22:51 UTC, about 14 min after planetary immersion. Just before emersion, at 00:15:40 UTC on 16 August, observations were restarted and continued to 03:36 UTC, at which time Uranus was at an air mass of 4.2. An offset guider was used to ensure that the photometer aperture remained centered on the (initially invisible) star. The diameter of the circular aperture was set at 10 arcsec for immersion and reduced to 7.5 arcsec for emersion. Because of this, and because of the decrease in sky background radiation at 2.2 μm as the Sun set, the signal-to-noise ratio of the post-emersion ring occultations is much better than that of the pre-immersion data. The weather at Las Campanas was mostly clear with some cirrus which, however, did not affect either the planetary or ring occultation observations.

Because of the high sky background level, and consequently noisy data, only the occultations by rings $\alpha, \beta, \gamma, \delta$, and ϵ are immediately apparent in the pre-immersion records. However, with the aid of the times reported by Bouchet *et al.* (1980), it has proven possible to identify occultations by rings 6, 5, and 4 as well. In the post-emersion records, occultations by all nine known rings are clearly visible. In Table I, the midtimes of the 17 identified ring occultations are given. The internal precision of these data is ± 0.1 s, and a correction of -0.1 s has been applied to allow for the delay in the recording system's response, estimated at ~ 70 ms. Systematic errors owing to poor synchronization with WWV or an incorrect strip chart pen offset should be less than ± 0.3 s.

In addition to the events in Table I, at least eight brief, shallow features appear in the post-emersion data. None of these coincides with any of events a–g of Bouchet *et al.*, and many have the appearance of instrumental "glitches" rather than genuine occultations by satellites or rings.

TABLE I. Midtimes of ring occultations, Las Campanas, 15/16 August 1980.

Ring	Pre-immersion 15 Aug. 1980, UTC	Post-emersion 16 Aug. 1980, UTC
6	22:11:17.0	00:45:57.7
5	22:10:21.4	00:46:49.7
4	22:09:50.7	00:47:30.6
α	22:05:25.4	00:51:51.2
β	22:03:27.4	00:53:41.9
η	—	00:56:41.2
γ	21:59:28.7	00:57:34.9
δ	21:58:07.2	00:58:55.1
ϵ	21:52:55.0	01:04:44.6

TABLE II. Observed and predicted mean delays between ring occultations at ESO, CTIO, and Las Campanas (LC), evaluated separately for pre-immersion (I) and post-emersion (E) events.

	ESO – LC		CTIO – LC	
	I	E	I[a]	E
Observed mean delay, Δt (s)	−0.07	0.61	−0.11	1.96
Predicted mean delay, Δt_p (s)	−0.25	0.41	−0.22	1.97
$\Delta t - \Delta t_p$ (s)	0.18	0.20	0.11	−0.01

[a]Rings γ and ϵ only.

As a check on the possible presence of systematic errors, a comparison may be made between the data in Table I and the occultation midtimes reported for ESO (Bouchet *et al.* 1980) and CTIO (Elliot *et al.* 1981a). The results of such a comparison are presented in Table II, as observed mean time delays for pre-immersion and post-emersion ring occultations, and the corresponding predicted mean delays based on the astrometric analysis in Sec. III. To allow for variations in the delays between the innermost and outermost rings (~ 1.5 s for CTIO – LC), the predicted delays are calculated for a hypothetical circular ring with a radius of 45 728 km, equal to the mean semimajor axis of the ring system (Elliot *et al.* 1981a). However, for the CTIO – LC pre-immersion comparison only γ- and ϵ-ring data are available, and the predicted delay is adjusted accordingly.

The comparison between CTIO and Las Campanas times indicates that no systematic error greater than 0.1 s exists between these two stations. The ESO – Las Campanas comparison, however, suggests the presence of a systematic error of ~ 0.2 s in one of these two data sets, in the sense that the ESO times are too late relative to the Las Campanas times. Based on these results, it appears unlikely that there is any systematic error in the data in Table I greater than 0.2 s.

III. OCCULTATION GEOMETRY

At the midtime of the occultation, $\sim$23:30 UTC, 15 August 1980, the inclination of the ring plane to the plane of the sky was 26°.734 and the position angle of the north pole of the ring plane, projected on the sky, was 268°.442, based on the elements of the pole given by Elliot *et al.* (1981a). As observed from Las Campanas, the center of Uranus passed ~ 0.95 arcsec to the south of the occulted star, with a mean topocentric velocity of 7.77 km s^{-1} in position angle 107°.13.

Positions of the occulting segments of the rings in the plane of the sky, relative to the center of Uranus, are calculated from the occultation midtimes in Table I in the manner described by Elliot *et al.* (1978). Apparent

TABLE III. Ring plane coordinates of the occulting ring segments.

Ring	Pre-immersion R (km)[a]	Pre-immersion θ[b]	Post-emersion R (km)[a]	Post-emersion θ[b]
6	418 45.3	169°.897	418 46.2	24°.451
5	422 99.0	170°.092	422 76.6	24°.266
4	425 49.7	170°.198	426 15.5	24°.122
α	447 22.1	171°.064	447 81.6	23°.259
β	456 91.3	171°.423	457 05.1	22°.917
η	—	—	472 04.6	22°.390
γ	476 57.0	172°.104	476 54.6	22°.239
δ	483 29.5	172°.325	483 27.3	22°.018
ϵ	509 12.0	173°.115	512 68.5	21°.121

[a] $\pm$ 3 km.
[b] $\pm$ 0°.003.

geocentric positions for Uranus are obtained by four-point Gaussian interpolation in the *Astronomical Ephemeris* tabulation of daily positions, and for the occulted star by application of precession, nutation, and aberration corrections to the 1950.0 position given by Klemola and Marsden (1977). The six available observations of occultations by the near-circular γ ring on 15/16 August 1980 are used to determine corrections to these sky plane positions, in order to account for errors in both the planetary ephemeris and the stellar position. Finally, the corrected sky plane positions are projected into the ring plane, and expressed in polar coordinates R (radius) and θ [azimuth, measured from the ascending (i.e., western) node of the ring plane on the Earth's equator of date]. A more complete description of this procedure is given by Nicholson *et al.* (1981).

Table III lists the ring plane coordinates corresponding to the 17 identified ring occultations observed at Las Campanas. These results are based on the ring plane orientation and semimajor axis for ring γ, a_γ, recently determined by Elliot *et al.* (1981a). Quoted uncertainties reflect timing uncertainties of $\pm$ 0.2 s, and possible errors due to approximations made in the calculations (see below), but do *not* incorporate uncertainties in either the ring plane pole position ($\pm$ 0°.05) or a_γ ($\pm$ 33 km).

The reduction procedure outlined above neglects certain refinements introduced by Elliot *et al.* (1981a) in their reanalysis of all available occultation data for the Uranian rings. The principal corrections, and the estimated maximum errors introduced into the present calculation of sky plane coordinates by their omission, are as follows: (1) allowance for the difference in light travel time from different parts of the rings ($\sim$0.6 km), (2) removal of stellar aberration from the apparent positions of Uranus and the star ($\sim$0.6 km), (3) use of the JPL DE96 ephemeris for Uranus rather than that given in the *Astronomical Ephemeris* (most of the effects of this change are absorbed in the corrections made to the sky plane coordinates; residual differential effects in the ring radii amount to a maximum of $\sim$1.1 km). The maximum cumulative error of $\sim$2.3 km in the calculated radii of ring segments is somewhat greater than the $\pm$ 1.6 km attributable to timing uncertainties of $\pm$ 0.2 s. In addition, the azimuths in Table III are referred to the ascending node of the ring plane on the Earth's equator of date. To correct them to the node on the equator of 20:00 UT, 10 March 1977, as used by Elliot *et al.* (1981a), they should be increased by 0°.019.

IV. RING OCCULTATION PROFILES

Measurements of fractional depth and FWHM duration for the ring occultations listed in Table I are presented in Table IV. Uncertainties in fractional depth are $\pm$ 0.1 and $\pm$ 0.02 for pre-immersion and post-emersion events, respectively, and uncertainties in duration are $\pm$ 0.02 s. As discussed in Sec. II, the post-emersion records are of much higher signal-to-noise ratio than those obtained prior to the planetary occultation, and the following discussion will largely be restricted to the post-emersion data. Also given in Table IV are the apparent widths of the rings, projected on the sky, and the inferred radial widths in the ring plane. Durations and fractional depths for the ring occultations observed at ESO are generally consistent with the data in Table IV, the largest discrepancies involving the post-emersion α and β events, for which Bouchet *et al.* (1980) reported durations of 1.2 and 1.5 s, respectively.

a) The Narrow Rings

In Figs. 1 and 2 are reproduced the segments of the post-emersion records of 16 August 1980 containing occultations by rings 6–δ. Contributions by Uranus and the rings to the 2.2-μm flux entering the 7.5-arcsec-diameter aperture amounted to less than 3% of the stellar flux, and may be neglected. Superimposed on the observed light curves are synthetic profiles discussed in Sec. IV c.

TABLE IV. Fractional depths and durations of ring occultations, Las Campanas, 15/16 August 1980.

Ring	Fractional depth	Duration (FWHM) (s)	Projected width (km)	Radial width (km)
		Pre-immersion		
6	0.3	0.33	2.4	2.7
5	0.4	0.51	3.8	4.2
4	0.4	0.43	3.2	3.5
α	0.7	0.61	4.5	5.0
β	0.5	0.87	6.4	7.2
γ	0.55	0.43	3.2	3.5
δ	0.65	0.63	4.6	5.2
ϵ	0.6–0.9	3.98	29.3	32.9
		Post-emersion		
6	0.22	0.39	3.0	3.3
5	0.38	0.39	3.0	3.3
4	0.34	0.44	3.4	3.7
α	0.57	1.09	8.4	9.1
β	0.32	1.26	9.7	10.5
η	0.23	0.45	3.5	3.8
γ	0.80	0.54	4.2	4.5
δ	0.67	0.43	3.3	3.6
ϵ	0.63–0.92	8.02	61.8	67.5

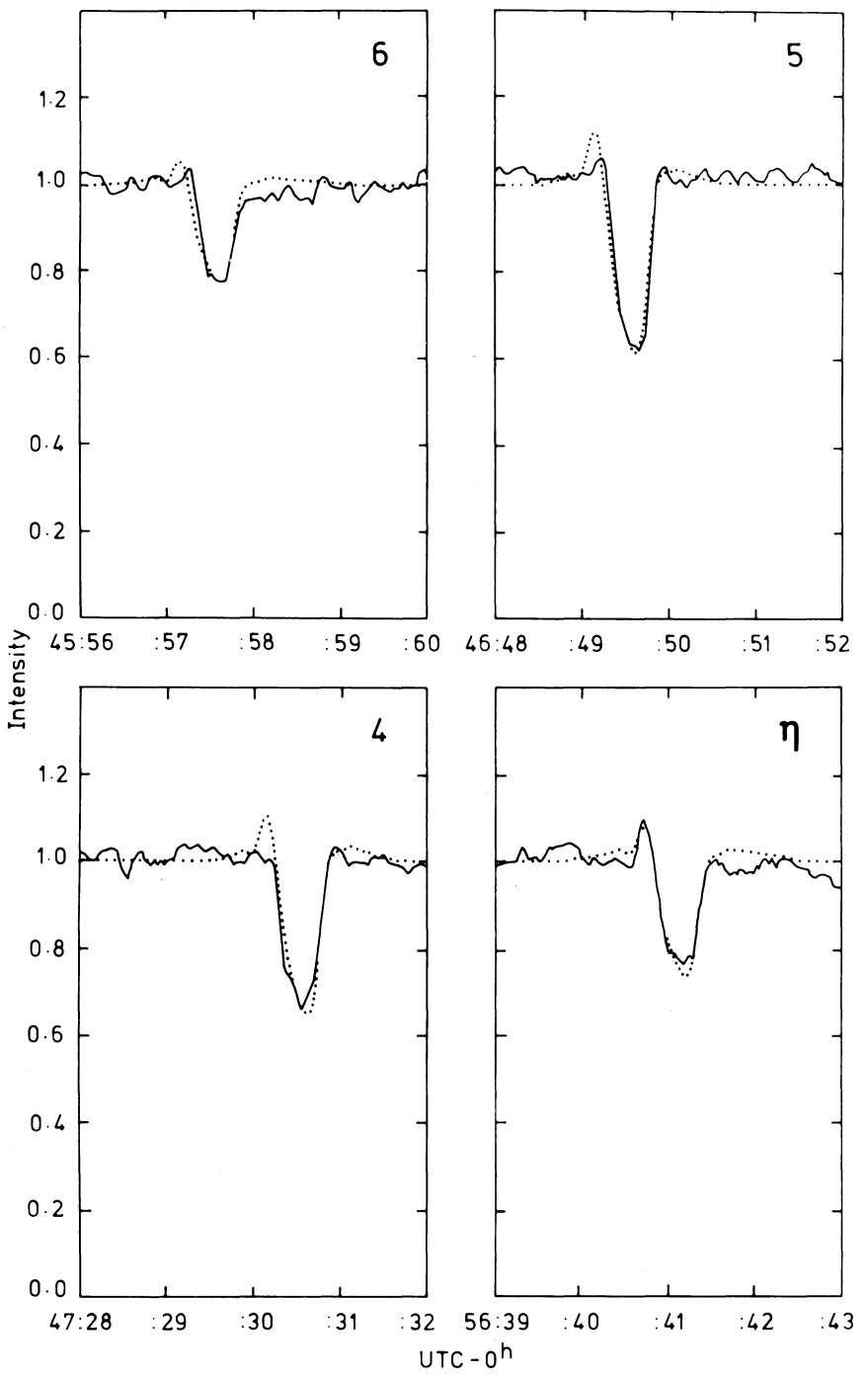

FIG. 1. Normalized post-emersion occultation light curves for rings 6, 5, 4, and η, observed at Las Campanas on 16 August 1980. The nonstellar component of the total flux is less than 3%. The dotted curves are synthetic occultation profiles corresponding to a stellar angular diameter of 1.3×10^{-4} arcsec, an instrumental time constant of 100 ms, and the ring widths and optical depths listed in Table VI. The secondary component of the η-ring event is shown in Fig. 3.

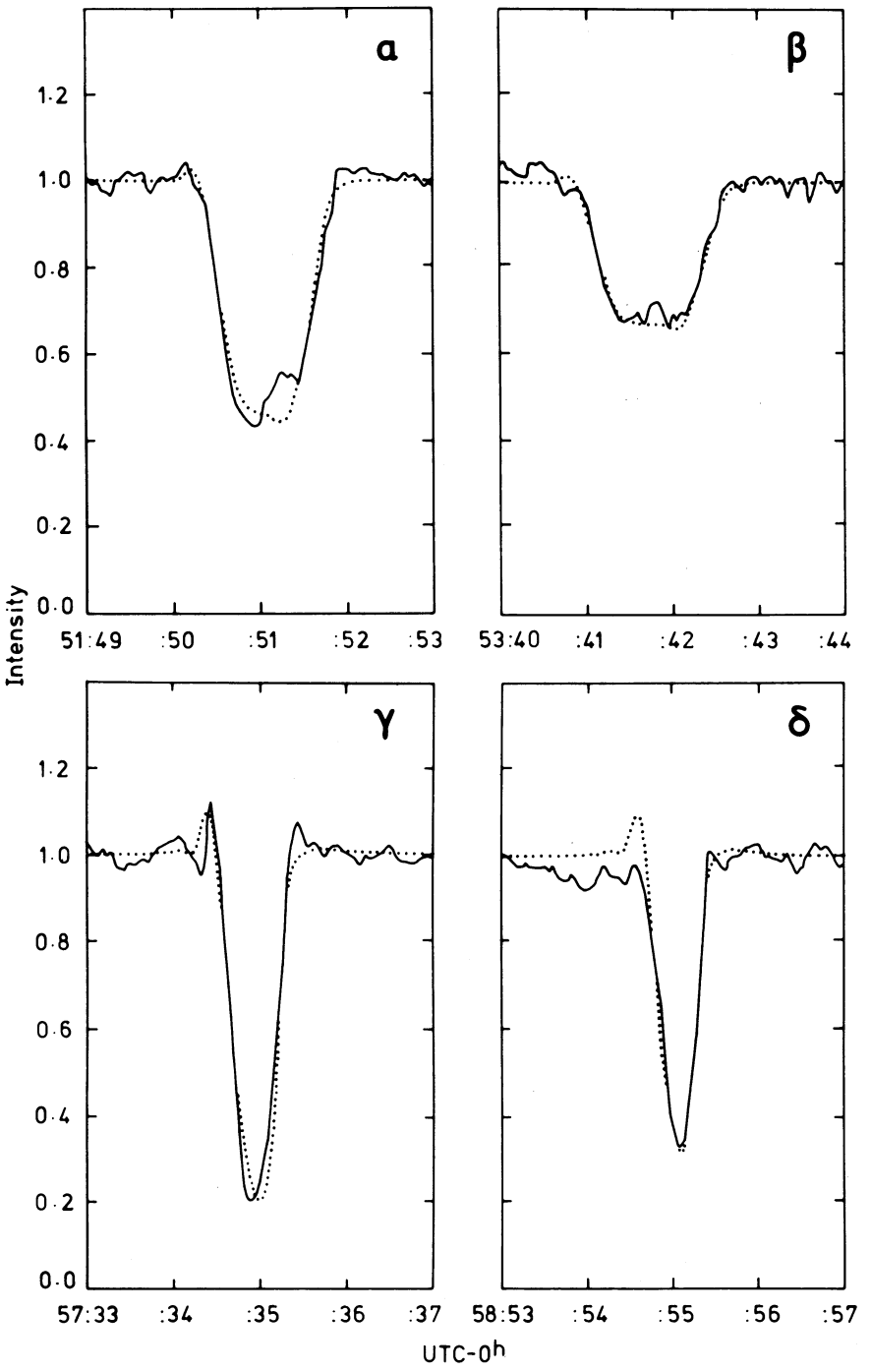

FIG. 2. Normalized post-emersion occultation light curves for rings α, β, γ, and δ. The dotted curves again represent synthetic occultation profiles corresponding to the models in Table VI. Features to be particularly noted include structure in the α profile, the diffraction "spike" leading the γ event, and the decrease in intensity preceding the δ event (see text).

The narrowest occultation profiles are exhibited by rings 6, 5, 4, η, and δ, with apparent projected widths of 3.0–3.5 km. This minimum width is set by diffraction [the Fresnel diffraction scale, $(2\lambda D)^{1/2} = 3.51$ km, for a wavelength $\lambda = 2.2\,\mu$m and a distance $D = 18.767$ AU]; the true widths of these rings may be considerably less, as shown below. Rings α, β, and γ, on the other hand, show significantly greater profile widths (4.2–9.7 km), and may be said to have been "resolved," although these profiles too have been strongly modified by diffraction. The α-ring profile shows definite evidence of internal structure, confirming similar reports by Sicardy (1981, private communication) and Elliot *et al.* (1981a). In light of the suggestion by the latter authors that this ring may consist of two closely spaced components, the mean optical depth determined below should be interpreted with caution. Hubbard and Zellner (1980) have also suggested that the α ring is nonuniform in structure, although the signal-to-noise ratio of their data was much lower.

Apart from broadening and smoothing the occultation profiles, diffraction is also responsible for the narrow positive spikes, or fringes, which precede the η and γ events, as is shown by the synthetic profiles. The events due to rings 6 and 5 may also show these diffraction fringes, although they are scarcely above the noise level in the data. Model calculations indicate that the symmetric trailing diffraction fringes are suppressed by the instrumental response, in agreement with the observations (see Fig. 5). The absence of significant fringes associated with the α and β events in Fig. 2 is consistent with a combination of instrumental smoothing and the comparatively low optical depths of these ring segments (see below). However, Elliot *et al.* (1981a), whose observations were obtained with a shorter time constant of 30 ms, also did not observe fringes associated with the post-emersion α event, and attributed this to unsharp ring edges.

An important result of the occultation observations of 15/16 August 1980 was the discovery of secondary components of low optical depth associated with rings η and δ (Elliot *et al.* 1981a). From Fig. 2, the secondary component of ring δ, located interior to the main ring, is estimated to have a radial width of ~ 13 km and an optical depth (at 2.2 μm) of ~ 0.05. The somewhat broader secondary component exterior to ring η is shown in Fig. 3, extending for a radial distance of ~ 55 km and terminated by a sharp spike. Although the width and location of this feature are in agreement with observations made at CTIO (Elliot *et al.*) and at ESO (Sicardy 1981, private communication), the apparent mean optical depth of ~ 0.03 is not. Figure 3 of Elliot *et al.* (1981a) shows an average extinction of $\sim 10\%$ of the incident stellar flux, or an optical depth of 0.1, while the ESO observations show an average extinction of $\sim 5\%$. These changes in the optical depth of the secondary component occur within an azimuthal distance of only 135 km, or 2.5 times its radial width.

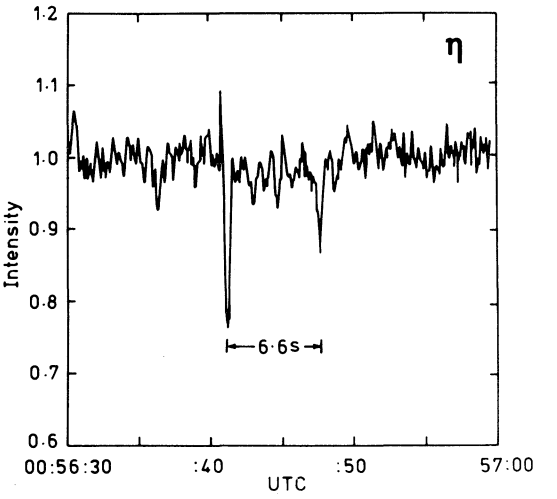

FIG. 3. The post-emersion η-ring occultation, showing the very shallow secondary component terminated by a sharp feature 6.6 s after the primary event. This interval corresponds to a radial separation of 55 km. Compare this light curve with Fig. 3 of Elliot *et al.* (1981a), which shows a drop in intensity of $\sim 10\%$ for ~ 6.3 s following the primary η event.

b) The ϵ Ring

Only the ϵ ring is sufficiently broad for the effects of diffraction to be unimportant in shaping the overall occultation profile. The post-emersion profile of 16 August 1980 is shown in Fig. 4, and corresponds to a radial

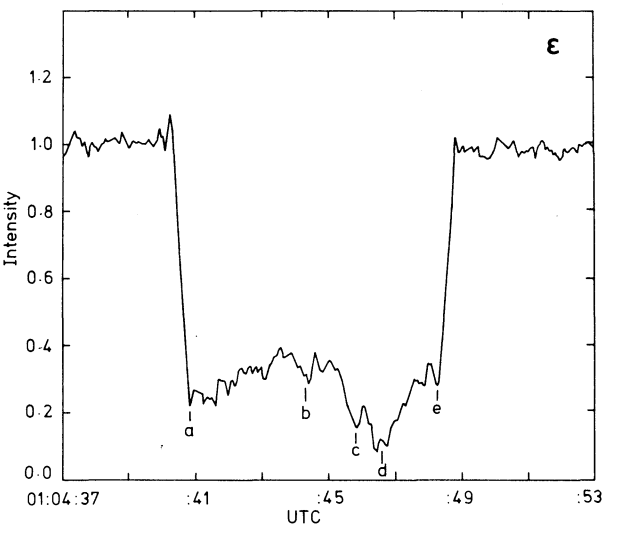

FIG. 4. Normalized post-emersion occultation light curve for ring ϵ. The FWHM duration of 8.02 s corresponds to a radial width of 67.5 km. Note the steeply sloping edges of the profile and the possible diffraction spike at the leading edge. Five optical depth maxima, *a–e*, are identified in this figure and their separations given in Table V. These features are also recognizable in most previously published profiles of the ϵ ring (see text).

width of 67.5 km, somewhat greater than the mean width for this ring of 59 km (Nicholson *et al.* 1981) but considerably less than the maximum width of 100 km. The internal structure of the ϵ ring revealed in this figure is essentially identical to that observed during previous occultations when the width of the occulting segment exceeded ~45 km. Narrower segments of this ring, however, exhibit relatively featureless profiles (Elliot *et al.* 1981b). This difference in optical depth profile between broader and narrower parts of the ring is consistent with the self-gravitating models studied by Goldreich and Tremaine (1979b), which show similar variations in surface density profile due to nonuniform radial eccentricity gradients across the ring.

In order to quantitatively define this characteristic structure of the broader section of the ring, and to facilitate comparison with previous observations, five optical depth maxima, *a–e*, are identified in Fig. 4. In Table V the spacings *ab*, *ac*, and *ad*, normalized so that *ae* = 1.0, are given for the present ϵ profile and the six published profiles with radial widths greater than 45 km. No systematic variation of the normalized spacings, either with ring segment width or with date of observation, is apparent in these data. With the single exception of the rather noisy pre-immersion profile of 10 June 1979, there is no difficulty in recognizing the structure of Fig. 4 in any of the published profiles.

Finally, we note that although neither diffraction nor instrumental time constant significantly affects the overall structure of the ϵ-ring occultation profile, they do limit the radial resolution to ~3 km. At higher resolution, such as may be achieved by occultation observations at visual wavelengths or by spacecraft imaging, it is possible that the structure in Fig. 4 will break up into a series of narrow subrings separated by gaps, as suggested by Goldreich and Tremaine (1981).

c) Synthetic Profiles

In order to determine ring segment widths and optical depths from the occultation profiles in Figs. 1 and 2, synthetic occultation profiles are generated for a variety of ring models. Each ring segment is modeled as an infinitely long bar of projected width W and uniform optical depth τ, at a distance of 18.767 AU from the observer. The diffraction pattern produced by this bar due to an infinitely distant point source of light is calculated for three wavelengths—2.07, 2.20, and 2.33 μm—and then averaged, to simulate the effect of the 0.4-μm bandpass of the observations. This spatial diffraction pattern is then convolved, first with the intensity distribution of the stellar source, modeled as a uniform disk of angular diameter 1.3×10^{-4} arcsec (Elliot *et al.* 1981a), and then with an instrumental response function $f(t)$. The velocity of the observer normal to the shadow of the ring is set at 7.5 km s^{-1}, a value representative of the 15/16 August 1980 occultation, and the impulse response function is taken to be

$$f(t) = t/t_0^2 e^{-t/t_0},$$

with a time constant t_0 of 100 ms. The multiplicative factor t/t_0^2 applies to a 12 db per octave rolloff filter, and is therefore not strictly applicable to the present observations (see Sec. II). However, its effect on the durations and fractional depths of the synthetic profiles is believed to be negligible, although the amplitudes of the diffraction fringes may be somewhat reduced. [The form of $f(t)$ was initially chosen in the belief that the lock-in amplifier *was* operated in the 12 dB per octave mode; subsequent investigations, including measurements of rise and fall times from the original strip chart, have indicated that this was not the case.] The successive stages in the generation of a synthetic profile are illustrated in Fig. 5, for an opaque ring of projected width 3 km.

In Fig. 6 are presented the results of a series of model calculations for 0.2 km $\leqslant W \leqslant$ 10 km and $0.2 \leqslant \tau \leqslant \infty$, in the form of a plot of fractional depth vs FWHM of the synthetic profiles. Although these results are derived for particular values of stellar angular diameter and instrumental time constant, further numerical calculations indicate that they are comparatively insensitive to these

TABLE V. Comparison of ϵ-ring profiles in terms of points *a–e* identified in Fig. 4.

Event[a]	ϵ radial width (km)	*ab*/*ae*	*ac*/*ae*	*ad*/*ae*	Ref.[b]
16 Aug. 1980 E	67.5	0.47	0.68	0.78	this work
10 Mar. 1977 I	101	0.40	0.64	0.78	1
10 Mar. 1977 I	94	0.39	0.68	0.82	2
23 Dec. 1977 I	47	0.43	—	0.73	3
10 Apr. 1978 E	76	0.44	0.64	0.82	4
10 Jun. 1979 I	75	(0.34)	(0.56)	(0.69)	5
10 Jun. 1979 E	51	0.33	0.66	0.82	5
Average (excl. 10/6/79 I)		0.41	0.66	0.79	

[a] I = pre-immersion, E = post-emersion.
[b] (1) Millis *et al.* (1977), (2) Bhattacharyya and Bappu (1977), (3) Millis and Wasserman (1978), (4) Nicholson *et al.* (1978), (5) Nicholson *et al.* (1981).

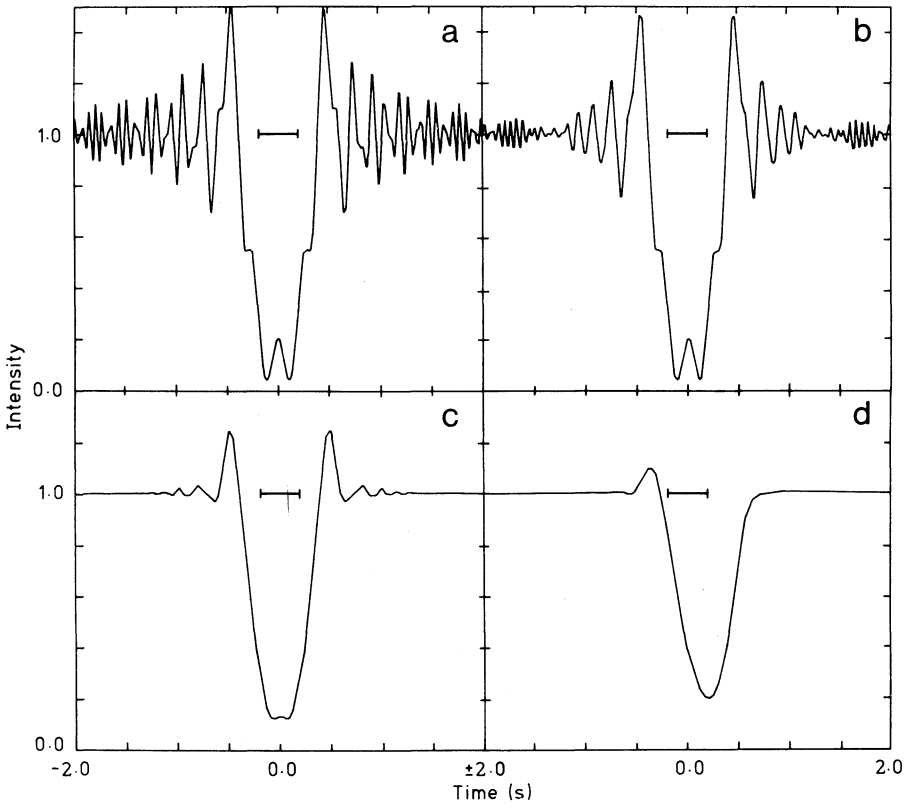

FIG. 5. Successive steps in the generation of a synthetic occultation profile for an opaque ring with a projected width of 3.0 km. The geometric shadow of the ring is indicated by a horizontal bar, and the velocity of the shadow relative to the observer is 7.5 km s^{-1}. (a) Monochromatic ($\lambda = 2.2$ μm) diffraction pattern for a point source, (b) averaged over the 2.0–2.4-μm passband, (c) convolved with the intensity distribution of a uniform circular source of angular diameter 1.3×10^{-4} arcsec, (d) convolved with the instrumental response function $f(t)$ with a time constant of 100 ms. This is the model for ring γ, shown in Fig. 2.

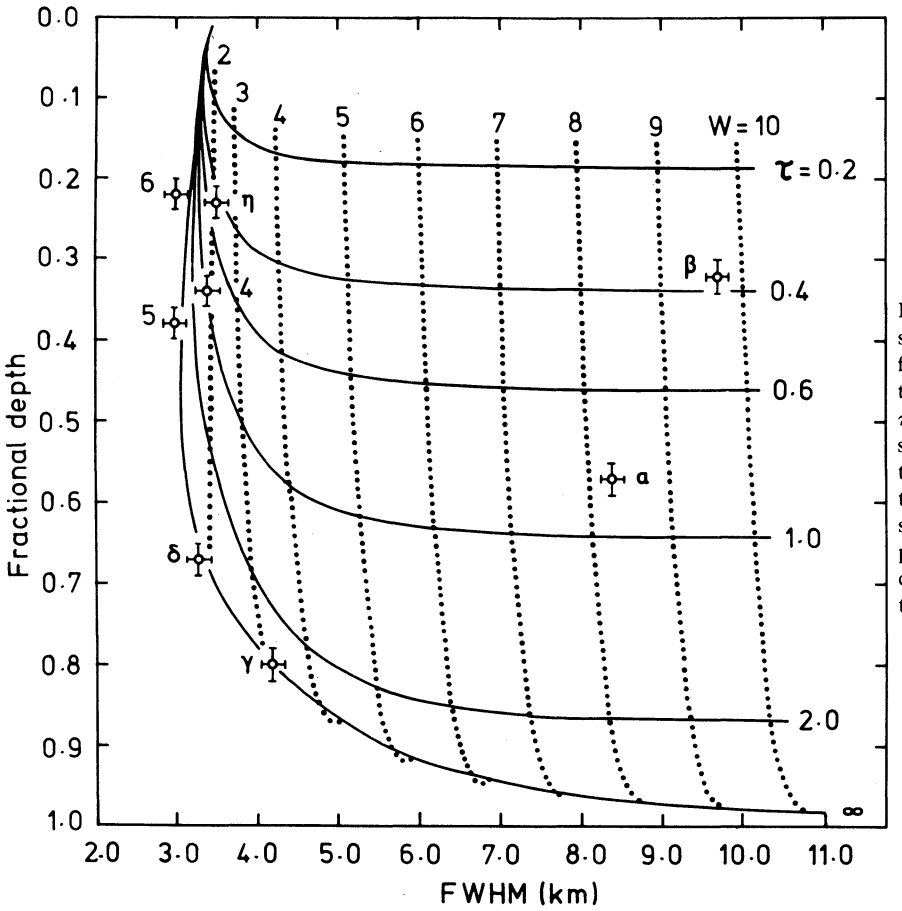

FIG. 6. Fractional depth vs FWHM for synthetic occultation profiles (see text for details). W is the projected width of the ring on the sky expressed in km, and τ is the line-of-sight optical depth, assumed uniform across the ring. Data for the post-emersion ring occultations are taken from Table IV. Note that the abscissa is the FWHM of the occultation profile as projected on the sky, not the corrected radial FWHM in the plane of the rings.

two parameters. Only for stellar diameters $> 3.6 \times 10^{-4}$ arcsec and/or time constants $> 150 \times (7.5/v)$ ms, where v is the shadow velocity in km s^{-1}, are the profile widths and depths significantly altered. Also plotted on this figure are the data for the post-emersion ring occultations of 16 August 1980, from Table IV.

For $W < 2$ km, irrespective of the value of τ, the FWHM is given approximately by the Fresnel diffraction scale of 3.5 km. In this regime, the fractional depth decreases with decreasing W and/or τ, and it is, in general, not possible to infer unique values of either parameter from an observed fractional depth. The present observations of rings 6, 5, and 4, and of the narrow component of ring η, fall in this indeterminate category. The observed fractional depths can, however, be used to set lower limits on the projected widths of these rings, for $\tau = \infty$, of 0.4, 0.8, 0.7, and 0.5 km, respectively. If, on the other hand, the projected widths are arbitrarily set at a maximum value of 2.0 km, then the fractional depths imply optical depths of 0.5, 1.0, 0.8, and 0.6, respectively. Ring models with intermediate combinations of W and τ, could, of course, satisfy the observations equally well. The much larger fractional depth of the δ-ring occultation is consistent only with an opaque ($\tau > 3$) ring of projected width 2.0 ± 0.5 km.

For $W > 3$ km, the FWHM increases approximately linearly with W, as shown by Elliot *et al.* (1981b), and is only weakly dependent on τ. The fractional depth, however, is almost independent of W and increases monotonically with increasing τ. Values of W and τ may therefore be inferred directly from the observed FWHM and fractional depth. From the post-emersion data for rings α, β, and γ, projected widths of 8.0, 9.5, and 3.0 km, respectively, are obtained with estimated uncertainties of ± 0.5 km. Optical depths are ~ 0.8 and ~ 0.4 for rings α and β, respectively, with uncertainties of ± 0.1, and > 3 for ring γ. The quoted uncertainties are based on a careful comparison of the observed occultation light curves with a range of synthetic profiles, and are believed to be more realistic than the somewhat smaller uncertainties suggested by the error bars on the points in Fig. 6. No attempt has been made to fit the observed profiles in a formal, least-squares sense.

Synthetic occultation profiles which best fit the observations of 16 August 1980 are shown superimposed on the observed light curves in Figs. 1 and 2. For rings 6, 5, 4, and η, the profiles correspond to narrow, opaque models, as these provide slightly better overall fits to the data than do wider, partially transparent models. Model parameters for each of these synthetic profiles are listed in Table VI, along with the corresponding radial ring segment widths and normal optical depths.

With the exception of the internal structure in the α-ring profile and the secondary components of rings η and δ, the synthetic profiles provide excellent fits to the observed light curves. This, of course, does not preclude the possibility of fine structure within the rings on a scale comparable to, or smaller than, the diffraction scale length of ~ 3.5 km.

V. WIDTH AND OPTICAL DEPTH VARIATIONS

Variations in the width and radius of the ϵ ring were noted at the time of the discovery of the Uranian rings (Elliot *et al.* 1977). Subsequent observations (Nicholson *et al.* 1978) showed this ring to be eccentric, with the width variations being interpreted in terms of an increase in eccentricity from the inner to the outer edge of the ring. Goldreich and Tremaine (1979b) demonstrated the necessity of such a positive eccentricity gradient, on the assumption that the ring's self-gravity was responsible for the suppression of differential precession. More recently, nonzero eccentricities have been established for rings 6, 5, 4, α, and β (Nicholson *et al.* 1981; Elliot *et al.* 1981a,b) and systematic width variations have been demonstrated for ring β (Elliot *et al.* 1981b).

A summary of published ring occultation radial widths (FWHM) and fractional depths is presented in Tables VII(a) and VII(b), including data from Elliot *et al.* (1977, 1978, 1981b), Millis and Wasserman (1978), Nicholson *et al.* (1978, 1981), and Bouchet *et al.* (1980). Such data from different occultations must be compared with caution, because of differing stellar angular diameters, instrumental time constants, and, most importantly, wavelengths of observation. The March and December 1977 events were observed at visible and near-infrared wavelengths, while subsequent observations have all been made at a wavelength of 2.2 μm.

None of rings 6, 5, 4, or η exhibits significant variations in either radial width or fractional depth. The

TABLE VI. Model parameters corresponding to the synthetic occultation profiles in Figs. 1 and 2.

Ring	Projected width W (km)	Radial width (km)	Apparent optical depth τ	Normal optical depth
6	0.4	0.44	∞	∞
5	0.8	0.87	∞	∞
4	0.7	0.76	∞	∞
α	8.0	8.7	0.8	0.71
β	9.5	10.3	0.4	0.36
η	0.5	0.54	∞	∞
γ	3.0	3.3	∞	∞
δ	2.0	2.2	∞	∞

TABLE VII(a). Radial widths of ring occultation profiles, 1977–1980 (km).

Event[a]		6	5	4	α	β	η	γ	δ	ϵ	Radial velocity (km s^{-1})
10 Mar. 1977	I				9.6	10.4				94	12.5
	E				6.7	5.8				39	12.5
23 Dec. 1977	I							~4	~4	47	31.3
10 Apr. 1978	I	5.2	4.4	4.4	5.2	12.1	4.4	5.2	4.4	22	17.4
	E		4.4	4.4	5.2	10.5	4.4	4.4	4.4	76	17.4
10 Jun. 1979	I				6.4	6.4		4.3	4.3	75	21.3
	E			6.4	12.8	6.4		4.3	4.3	51	21.3
20 Mar. 1980	I[b]				7.6	5.2		4.0	5.5	25.4	variable
	I[c]					6.6				22.7	variable
	E[c]							4.0	3.3	28.4	variable
15/16 Aug. 1980	I[d]	4.1	4.1	3.3	4.5	6.6	3.3	4.1	4.1		8.2
	I[e]	2.7	4.2	3.5	5.0	7.2		3.5	5.2	32.9	8.2
	E[d]	3.8	3.3	3.3	10.0	12.5	3.8	5.0	3.8	67.7	8.4
	E[e]	3.3	3.3	3.7	9.1	10.5	3.8	4.5	3.6	67.5	8.4
Average		3.8	4.0	4.1	7.5	8.4	3.9	4.3	4.3	49.9	

[a]I = pre-immersion, E = post-emersion.
[b]SAAO observations.
[c]CTIO observations.
[d]ESO observations.
[e]Las Campanas observations (this work).

unusual width of 6.4 km obtained for ring 4 on 10 June 1979 is probably atttributable to noise in the data. For each of these four rings, the average radial FWHM of ~4.0 km, which corresponds to a projected width of ~3.6 km, is determined by diffraction (see Fig. 6). As the average fractional depths do not differ greatly from those of the present observations, the limits on intrinsic width and optical depth derived in Sec. IV c may be considered to apply to the rings as a whole. These limits, of course, still permit significant variations in width, up to a maximum of ~2 km, provided that they are accompanied by appropriate variations in optical depth.

For rings γ and δ, more data are available and somewhat greater variations occur, particularly in fractional depth. There are no marked correlations between FWHM and fractional depth, but it is of interest that the γ ring showed increases in *both* parameters between pre-immersion and post-emersion observations on 15/16 August 1980. Since both of these rings are very nearly, if not exactly, circular (Elliot *et al.* 1981a), variations in width and optical depth are unexpected; it is possible that the observed variations are largely due to the effects of different stellar angular diameters and instrumental time constants. In the case of the 10 March 1977 occultation of SAO 158687, whose apparent linear diameter at the distance of Uranus is ~5.5 km (Hubbard and Zellner 1980), the former is certainly important.

The average radial FWHM of 4.3 km and the average fractional depth of ~0.6 for each of γ and δ imply common values for intrinsic radial width and normal optical depth of ~3.3 km and ~1.5, respectively. These results differ somewhat from the model parameters derived from the present observations alone, which show the width of ring δ to be ~2.2 km and both rings to have optical depths > 3. Resolution of this matter, and of the question of the reality of the apparent-width variations, must await further observations of a quality comparable to those of Fig. 2.

TABLE VII(b). Fractional depths of ring occultation profiles, 1977–1980.

Event[a]		6	5	4	α	β	η	γ	δ
10 Mar. 1977	I				0.53	0.40		0.37	0.47
	E				0.49	0.33		0.39	0.39
23 Dec. 1977	I							0.8	0.8
10 Apr. 1978	I	0.2	0.35	0.25	0.6	0.4	0.2	0.7	0.5
	E		0.35	0.25	0.75	0.4	0.2	0.75	0.55
10 Jun. 1979	I				0.7	0.5		0.5	0.4
	E			0.4	0.6	0.5		0.4	0.6
15/16 Aug. 1980	I[b]	0.24	0.32	0.31	0.74	0.54	0.17	0.54	0.71
	I[c]	0.3	0.4	0.4	0.7	0.5		0.55	0.65
	E[b]	0.24	0.47	0.35	0.60	0.35	0.27	0.89	0.71
	E[c]	0.22	0.38	0.34	0.57	0.32	0.23	0.80	0.67
Average		0.25	0.38	0.33	0.63	0.42	0.21	0.61	0.59

[a]I = pre-immersion, E = post-emersion.
[b]ESO observations.
[c]Las Campanas observations.

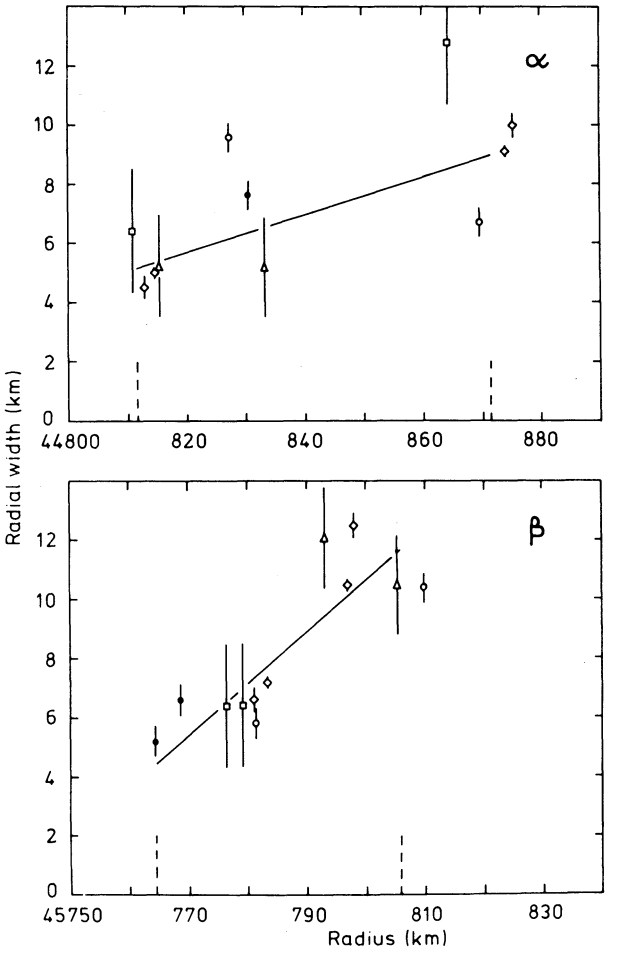

FIG. 7. Relations between radial width (FWHM) and radius in the ring plane for rings α and β. Note that these published radii are based on Dunham's (1971) pole, and must be decreased by $\sim$91 km to bring them into agreement with the pole of Elliot *et al.* (1981a). Periapse and apoapse for each ring, corresponding to the eccentricities in Table IX, are indicated by dashed lines. Weighted least-squares fits to the data are shown as solid lines. Key: open circles = 10 March 1977, triangles = 10 April 1978, squares = 10 June 1979, closed circles = 20 March 1980, diamonds = 15/16 August 1980.

In contrast, width variations are definitely established for rings α, β, and ϵ. Observed radial widths for both α and β range from $\sim$5 to $\sim$12 km, and for both rings there exist negative correlations between FWHM and fractional depth. Published measurements of FWHM radial width and radius, plus those obtained at Las Campanas and ESO on 15/16 August 1980, are plotted in Fig. 7 for each ring. Error bars on the points correspond to uncertainties in duration of $\pm$ 0.02 s (August 1980 LC), $\pm$ 0.05 s (August 1980 ESO), or $\pm$ 0.1 s (April 1978 and June 1979). Data for the March 1977 and March 1980 occultations were obtained from Elliot *et al.* (1981b), and assigned nominal uncertainties of $\pm$ 0.5 km. Similar plots were presented by Elliot *et al.* (1981b), but with only five and six points, respectively, against the present 11 and 12.

The width-radius relations displayed in Fig. 7 are qualitatively similar to that previously established for the ϵ ring, revised here in Fig. 8, and may likewise be interpreted in terms of increases in eccentricity from the inner to the outer edges of the rings. From the least-squares-fitted linear relations in Figs. 7 and 8, using Eqs. (1)–(4) of Nicholson *et al.* (1981), we obtain the total ranges in semimajor axis, $2\Delta a$, and eccentricity, $2\Delta e$, given in Table VIII. Mean values for a and e are taken from the elliptical models presented in Sec. VI. The results for rings β and ϵ are consistent with those obtained by Elliot *et al.* (1981b), while for ring α a considerably larger range in eccentricity is found, attributable to the increased number of data used in the fit. Note that the fitted values of $2\Delta a$, which represent the mean FWHM radial widths of the rings, are quite close to the averages of the observed widths given in the last line of Table VII(a).

With the aid of the width-radius relations in Fig. 7, the fractional depths in Table VII(b), and the theoretical results in Fig. 6, it is possible to estimate the true ranges of intrinsic radial width and normal optical depth for α and β. For ring α, the intrinsic width varies from $\sim$4.5 km at periapse to $\sim$9.0 km at apoapse, with a corresponding variation in normal optical depth from $\sim$1.6

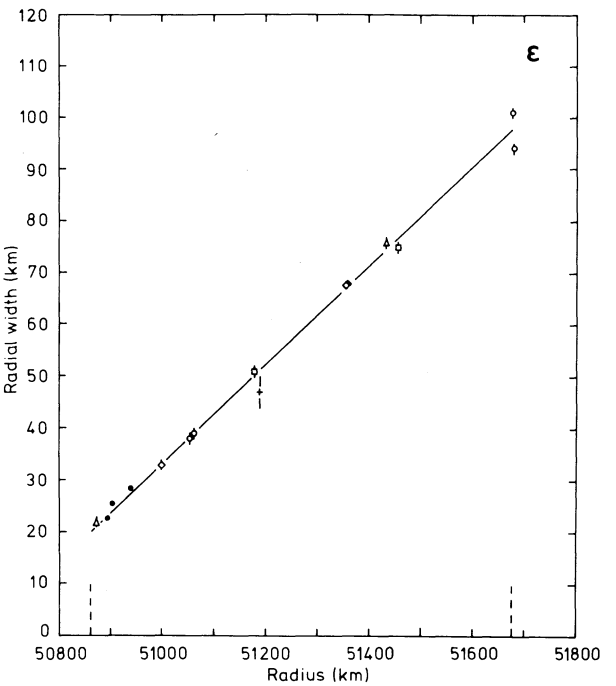

FIG. 8. Relations between radial width (FWHM) and radius in the ring plane for the ϵ ring. Note that these published radii are based on Dunham's (1971) pole, and must be decreased by $\sim$91 km to bring them into agreement with the pole of Elliot *et al.* (1981a). Periapse and apoapse, corresponding to the eccentricity in Table IX, are indicated by dashed lines. The solid line is a weighted least-squares fit to the 16 data points. Symbols are as for Fig. 7, except for the cross, which represents the 23 December 1977 observation.

TABLE VIII. Ranges in semimajor axis and eccentricity for rings α, β, and ϵ calculated from the relations in Figs. 7 and 8.

Ring	Range of semimajor axis,[a] $2\Delta a$ (km)	Range of eccentricity,[a] $2\Delta e$ (10^{-5})
α	7.1 ± 0.1	4.3 ± 0.3
β	8.1 ± 0.1	7.9 ± 0.5
ϵ	59.3 ± 0.1	74.9 ± 0.4

[a]With respect to values of a and e given in Table IX.

to $\sim$0.8. The optical depth is thus approximately inversely proportional to the radial width, consistent with a constant linear density of material around the ring. Similarly, ring β varies in intrinsic width from $\sim$3.5 km at periapse to $\sim$11.5 km at apoapse, with a corresponding variation in normal optical depth from $\sim$1.5 to $\sim$0.4. By chance, both the α and β occultation profiles in Fig. 2, and therefore the models in Table VI, refer to the widest and least opaque parts of these two rings.

Unfortunately, the greater optical depth combined with the often uncertain level of background (i.e., nonstellar) flux in occultation records makes such an examination of optical depth variations for the ϵ ring more difficult. There is, however, some evidence that the mean optical depth of this ring is also inversely proportional to its radial width (Elliot *et al.* 1978; Nicholson *et al.* 1978).

The eccentricity gradients derived above for rings α and β may be used to estimate the masses of these two rings, on the assumption that self-gravity is responsible for the suppression of differential apsidal precession. Using the approximate relation derived by Goldreich and Tremaine (1979a), and the data in Table VIII, we obtain masses of 5.0×10^{16} and 2.5×10^{16} g for α and β, respectively. The corresponding mean surface densities are 2.5 and 1.1 g cm^{-2}. Elliot *et al.* (1981b) have estimated the mass of ring β as 4×10^{16} g. These figures may be compared with a more carefully determined mass and mean surface density for the ϵ ring of 5×10^{18} g and 25 g cm^{-2} (Goldreich and Tremaine 1979b).

We complete our discussion of width variations by estimating the average integrated width of the entire system of nine rings. For rings α, β, γ, δ, and ϵ, average radial widths of 6.8, 7.5, 3.3, 2.2, and 59.3 km are adopted, respectively, while the width of each of rings 6, 5, 4, and η is assumed to lie in the range 0.6–2.2 km. The azimuthally averaged, integrated radial width of the ring system is then 85 ± 3 km and the total surface area is $(2.64 \pm 0.08) \times 10^7$ km^2. The rings therefore present a maximum projected area which is only 1.3% of the area of Uranus' visible disk, assumed to have an equatorial radius of 25 700 km (Elliot *et al.* 1981a).

VI. ELLIPTICAL RING MODELS

The eccentricity of the ϵ ring was established by Nicholson *et al.* (1978), who also determined its rate of apsidal precession due to the oblateness of Uranus. Subsequent occultation observations led to the construction of similar precessing elliptical models for rings 4, α, and β (Nicholson *et al.* 1981; Elliot *et al.* 1981b). For each of these models, it was assumed that the ring plane coincided with the orbital plane of the Uranian satellites, as given by Dunham (1971). Following the occultation of 15/16 August 1980, Elliot *et al.* (1981a) combined all of the available occultation data in a solution for the semimajor axes, eccentricities, and apsidal precession rates of all nine rings, and for the orientation of the ring plane. Rings 6 and 5 were also found to be eccentric, and ring δ possibly so. Upper limits of $\sim 1.2 \times 10^{-4}$ were established for the eccentricities of rings γ and η. The best-fitting pole of the ring plane was found to be displaced $\sim$0°.2 from Dunham's (1971) pole, which resulted in a systematic decrease of $\sim$91 km in the ring semimajor axes. The residual uncertainties of $\pm \sim$33 km in the semimajor axes are largely due to the remaining uncertainty of $\pm \sim$0°.05 in the pole position.

Further constraints on the pole position may come from an analysis of occultation radii for Uranus obtained on 10 March 1977, 10 June 1979, and 15/16 August 1980. The derived radii depend indirectly on the assumed ring pole, as the ring occultations are used to locate the apparent track of the occulted star relative to the center of Uranus. Preliminary results indicate that the use of Dunham's (1971) pole leads to unacceptably large ($\sim$80 km) radius residuals from any oblate spheroidal model for the planet, but that these residuals are much reduced when the pole of Elliot *et al.* (1981a) is used. The latter is thus to be preferred over the former.

As an independent check on the models of Elliot *et al.* (1981a), and for purposes of comparison with earlier models, we present in Table IX elliptical elements for rings 6, 5, 4, α, β, and ϵ. These models are based on essentially the same data set as that used by Elliot *et al.* (1981a), but with the addition of the Las Campanas observations of 15/16 August 1980. The model-fitting procedure has been described by Nicholson *et al.* (1981). No attempt has been made to redetermine the direction of the ring plane pole; the semimajor axes, which are the only ring parameters strongly sensitive to the pole, have been adjusted to be consistent with the pole of Elliot *et al.*

Before a comparison is made between the present elements and those of Elliot *et al.* (1981a), it is advisable to consider differences in the fitting procedures and their likely effects on the models.

(1) The present calculation of ring plane coordinates from occultation timing data is deficient in several respects, as discussed in Sec. III. Maximum errors in radius are estimated at $\pm$ 3 km.

(2) We fit elliptical models to ring plane coordinates which are calculated separately for each occultation, the coordinates for the March 1977 and March 1980 events being taken from Elliot *et al.* (1981b), and the remainder from Nicholson *et al.* (1981) and the present analysis of

TABLE IX. Elliptical elements for rings 6, 5, 4, α, β, and ϵ.

Ring	Semimajor axis[a] a (km)	Eccentricity e (10^{-3})	Azimuth of periapse[b] $\tilde{\omega}_0$	Apsidal precession rate $\dot{\tilde{\omega}}$ (deg day^{-1})	No. of data	rms deviation (km)
6	41 866	1.390 ± 0.022	$224.^{\circ}8 \pm 1.^{\circ}5$	2.7695 ± 0.0013	8	1.0
5	42 268	1.762 ± 0.050	$186.^{\circ}6 \pm 3.^{\circ}1$	2.6622 ± 0.0028	9	2.5
4	42 600	1.230 ± 0.097	$120.^{\circ}4 \pm 3.^{\circ}1$	2.5958 ± 0.0041	11	3.7
α	44 751	0.665 ± 0.028	$336.^{\circ}7 \pm 4.^{\circ}6$	2.1828 ± 0.0059	17	3.3
β	45 694	0.450 ± 0.026	$225.^{\circ}1 \pm 5.^{\circ}3$	2.0321 ± 0.0055	17	2.5
ϵ	51 180	7.941 ± 0.031	$215.^{\circ}3 \pm 0.^{\circ}4$	1.3624 ± 0.0004	16	3.2

[a]Adjusted to be consistent with the ring pole of Elliot *et al.* (1981a) (see text). Systematic uncertainties in a are $\pm \sim 33$ km, while relative uncertainties are $\pm \sim 4$ km.
[b]At 2000 UT, 10 March 1977 = JD 244 3213.33.

the August 1980 event. Since all of the earlier analyses have used Dunham's (1971) pole, our models are also calculated for this pole. In order to correct the models to the pole of Elliot *et al.* (1981a), all ring semimajor axes are reduced by 91 km from their fitted values. Errors introduced by this procedure, in comparison with a complete reanalysis of all previous raw occultation data as undertaken by Elliot *et al.* (1981a), are estimated at ± 2 km in the semimajor axes and $\pm 0.^{\circ}5$ in the azimuths of periapse.

(3) The present models minimize radius residuals, whereas those of Elliot *et al.* minimize occultation timing residuals. Although this results in a different weighting of the data used in the fit, it is not expected to systematically affect the results. Elliot *et al.* (1981a) obtained a mean radius residual of 0.02 km, very close to our value of zero.

(4) For the present models, each ring is treated independently of the others, there being no assumed relation between the apsidal precession rates. Elliot *et al.* (1981a), on the other hand, fit all of the rings simultaneously, requiring the precession rates to be consistent with fitted values for Uranus' gravitational moments J_2 and J_4. This distinction is important and will be discussed further below.

(5) Ring plane azimuths, in the present analysis, are referred to the ascending node of the ring plane on the Earth's equator of date, which slowly shifts in inertial space owing to the Earth's precession. Elliot *et al.* use the node on the equator of 20:00 UT, 10 March 1977 as a fixed reference point. The node has advanced $0.^{\circ}019$ in azimuth between this reference epoch and 16 August 1980, introducing a negligible error of -1.54×10^{-5} deg day^{-1}, into the apsidal precession rates in Table IX. As the azimuths of periapse refer to this same reference epoch, they are unaffected by precession.

With the exception of point (4) above, the cumulative effects of these modeling differences, due largely to approximations inherent in the present analysis, amount to ± 4 km in the semimajor axes and $\pm 0.^{\circ}5$ in the azimuths of periapse. No appreciable effects on either the eccentricities or the apsidal precession rates are anticipated.

When the elements in Table IX are compared with those in Table II of Elliot *et al.* (1981a), the agreement is found to be excellent with regard to the semimajor axes and eccentricities (recall, however, that the present semimajor axes have been uniformly adjusted to correspond with Elliot *et al.*'s pole, so that the present agreement does not reduce the ± 33-km systematic uncertainties quoted by Elliot *et al.*). The maximum discrepancy in semimajor axis is 2 km (rings 6, 5, and 4), somewhat less than might be expected. The only significant discrepancy in eccentricity involves ring α, for which Elliot *et al.* obtained $(0.72 \pm 0.03) \times 10^{-3}$, two standard deviations above the value in Table IX. Expressed as a difference in periapse or apoapse radius, this discrepancy amounts to only 2.5 km, less than the rms deviation of points from the model.

Agreement between the individually fitted apsidal precession rates in Table IX and those obtained by Elliot *et al.* from their fitted J_2 and J_4 is quite satisfactory for rings 4, α, β, and ϵ, the largest discrepancy being $+0.0033$ deg day^{-1} for ring β, or 0.6 standard deviations. For rings 5 and 6, the discrepancy increases to -0.0056 and $+0.0095$ deg day^{-1}, respectively. However, this appears to be due to a deviation of these two rings from their expected precession rates, since a second solution carried out by Elliot *et al.* (1981a), in which the precession rates were allowed to vary independently, yielded rates for rings 5 and 6 that differ by only 0.0008 and 0.0011 deg day^{-1}, respectively, from those in Table IX. Elliot *et al.* (1981a) have pointed out that this apparent deviation might be due to unmodeled dynamical effects, or to slight inclinations ($\lesssim 3^{\circ}$) relative to the other rings. When all the precession rates in Table IX are compared with the individually fitted rates obtained by Elliot *et al.*, the α and β rings show the greatest discrepancies, viz., $+0.0043$ and $+0.0049$ deg day^{-1}, respectively, or less than one standard deviation.

Because the azimuths of periapse are referred to the date of the first observed stellar occultation by Uranus, they are highly correlated with the apsidal precession rates. The large discrepancies in this quantity shown by rings 5 and 6 ($+4.^{\circ}8$ and $-11.^{\circ}1$, respectively) are attributable to the deviations in precession rate noted

above. When the models with individually fitted rates are compared (J. L. Elliot 1981, private communication), the discrepancies are reduced to $-1.^{\circ}0$ and $-0.^{\circ}2$, respectively, well within the formal errors. Similarly, the discrepancy for ring α is reduced from $+5.^{\circ}3$ to $+1.^{\circ}7$. The only remaining unexplained discrepancy is that of $-6.^{\circ}5$ for ring β, which is virtually unaffected by allowing the precession rate to "float" independently. Note, however, that because of the β ring's low eccentricity, a shift of 7° in the azimuth of periapse translates into a maximum radial discrepancy between the models of only 2.5 km.

It is concluded that the present elliptical models for rings 6, 5, 4, α, β, and ϵ are consistent with, and therefore confirm, the results of Elliot *et al.* (1981a). Those differences that do exist are, for the most part, smaller than the formal errors derived from the least-squares solutions and result in predicted ring radii which differ by less than ± 3 km. Radial variations of this magnitude are anticipated, owing to the approximations inherent in the present calculations and the differences in fitting procedure outlined above. The apparent deviations of the apsidal precession rates for rings 5 and 6 from their expected values are confirmed, although it is noted that there exist fewer data for these two rings than for any of the others; it is conceivable that further observations will force significant changes in the model precession rates. In connection with ring 6, we confirm the observation of Elliot *et al.* (1981a) that the April 1978 emersion datum is quite inconsistent with the remaining data, and must be rejected. This event was only just above the noise in the occultation record (see Nicholson *et al.* 1978), and was evidently misidentified.

A brief comparison of the present models of rings 4, α, β, and ϵ with those of Nicholson *et al.* (1981) is in order. The principal improvement, apart from the correction of semimajor axes to reflect Elliot *et al.*'s (1981a) determination of the ring pole, lies in the elimination of model "4b" for ring 4, and the confirmation of model "4a," as anticipated on the basis of their apsidal precession rates. The only other significant changes concern ring α, whose eccentricity has been increased by $\sim 10\%$, and whose precession rate has been reduced, bringing it into much better agreement with the rate predicted from Uranus' J_2. Of course, the inclusion of data from two further occultations (20 March and 15/16 August 1980) has led to a considerable reduction in the standard errors of all elements.

As part of their solution for the orbital elements of the nine rings, Elliot *et al.* (1981a) obtained values for Uranus' zonal gravity harmonic coefficients of

$$J_2 = (3.352 \pm 0.006) \times 10^{-3}$$

and

$$J_4 = (-2.9 \pm 1.3) \times 10^{-5},$$

for an equatorial planetary radius of 26 200 km. As mentioned above, individually fitted apsidal precession rates for rings 4, α, β, and ϵ were quite consistent with these values, although the rates for rings 5 and 6 were not.

From a weighted least-squares fit* of Eq. (6) of Nicholson *et al.* (1981) to the data in Table IX, we obtain

$$J_2 = (3.347 \pm 0.008) \times 10^{-3}$$

$$J_4 = (-3.6 \pm 1.2) \times 10^{-5},$$

with the above equatorial radius. The adopted mass of Uranus,

$$GM = 5.784\,18 \times 10^6 \text{ km}^3 \text{ s}^{-2}$$

(Nicholson *et al.* 1981), differs slightly from the value used by Elliot *et al.* (1981a), $5.782\,22 \times 10^6$ km^3 s^{-2}. This result is in satisfactory agreement with that of Elliot *et al.* (1981a), although the value of J_4 is rather sensitive to the weighting of the data for rings 5 and 6. Residuals from the above fit for these two rings are -0.0079 and 0.0080 deg day^{-1}, respectively, much greater than the formal uncertainties in Table IX. If rings 5 and 6 are omitted from the fit entirely, we obtain

$$J_2 = (3.350 \pm 0.011) \times 10^{-3}$$

and

$$J_4 = (-3.1 \pm 1.7) \times 10^{-5},$$

essentially the same as Elliot *et al.*'s (1981a) result. It is noted that all of the above values for J_4 lie in the probable range suggested by Nicholson *et al.* (1981) of $(-4.6$ to $-2.3) \times 10^{-5}$, based on a comparison with Jupiter, Saturn, and Neptune.

The decrease in J_2 from previous estimates of $\sim 3.390 \times 10^{-3}$ (Nicholson *et al.* 1981; Elliot *et al.* 1981b) is due, in approximately equal proportions, to the 91-km decrease in ring semimajor axes and to the nonzero value obtained for J_4.

VII. CONCLUSIONS

(1) Occultations by the nine Uranian rings—6, 5, 4, α, β, η, γ, δ, and ϵ—were observed at Las Campanas on 15/16 August 1980. Events a–g reported by Bouchet *et al.* (1980) are not confirmed. Rings η and δ are found to have secondary components of low optical depth and with radial widths of 55 and ~ 13 km, respectively, in confirmation of a similar report by Elliot *et al.* (1981a).

(2) The post-emersion occultation profile of the ϵ ring, with a radial width of 67.5 km, is compared with six previous ϵ profiles with widths ranging from 47 to 101 km (Table V). A consistent internal structure is described, with no significant changes having occurred in the structure of this ring during a period of over 3 yr.

(3) Synthetic occultation profiles are generated to match the observations of rings 6, 5, 4, α, β, η, γ, and δ (Figs. 1 and 2, Table VI). These models include the effects of diffraction, spectral bandpass of the observa-

*In order to prevent their dominating the fit, the uncertainties in precession rate for rings 4, 5, and 6 were arbitrarily increased to 0.005 deg day^{-1}, comparable with those for rings α and β.

tions, stellar angular diameter, and instrumental response, and provide generally good fits to the observed profiles. In addition, results are given for a grid of model rings with projected widths between 0.2 and 10 km and optical depths between 0.2 and ∞ (Fig. 6).

(4) The durations of occultations by rings 6, 5, 4, and η are controlled by diffraction, and do not reflect the true widths of these narrow rings. Occultation fractional depths provide constraints on the widths W and optical depths τ, but do not yield unique models. The range of models consistent with the observations of ring 4, for example, extends from $W = 0.7$ km, $\tau = \infty$ to $W = 2$ km, $\tau = 0.8$. Similar results are obtained for rings 6, 5, and η.

(5) Rings α and β exhibit significant width variations and inversely correlated variations in occultation fractional depth [Tables VII(a) and VII(b)]. Correlations between width and radius for these two rings are confirmed, and interpreted in terms of eccentricity gradients across the rings (Fig. 7 and Table VIII). According to models fitted to the available data, ring α varies in width from ~ 4.5 to ~ 9.0 km, while the range for ring β is ~ 3.5 to ~ 11.5 km. In each case, the ring is widest at apoapse and narrowest at periapse, with the optical depth being approximately inversely proportional to the radial width.

(6) The near-circular rings γ and δ also show some evidence of width and/or optical depth variations, but this may be an artifact of variations in occultation parameters such as stellar angular diameter. Average radial widths and optical depths for γ and δ appear to be ~ 3.3 km and ~ 1.5, although the present observations suggest that both rings are opaque and that the radial width of ring δ is only ~ 2.2 km.

(7) The width-radius relation for the ϵ ring is revised slightly to incorporate the present observations (Fig. 8 and Table VIII).

(8) On the assumption that differential apsidal precession is prevented by the rings' self-gravity, approximate masses of 5.0×10^{16} and 2.5×10^{16} g are obtained for α and β, respectively, corresponding to mean surface densities of 2.5 and 1.1 g cm^{-2}.

(9) The azimuthally averaged, integrated radial width of the nine Uranian rings is 85 ± 3 km, and their total surface area is $(2.64 \pm 0.08) \times 10^7$ km^2.

(10) Elliptical models derived for rings 6, 5, 4, α, β, and ϵ from the available occultation data are consistent with, and confirm, the results of Elliot *et al.* (1981a). In particular, it is found that the apsidal precession rates obtained for rings 5 and 6 cannot be reconciled with the values of Uranus' J_2 and J_4 derived from observations of the remaining four elliptical rings.

The authors gratefully acknowledge the assistance of the staff of the Las Campanas Observatory in making the observations. The discussion in Sec. VI has benefited considerably from a detailed critique by J. L. Elliot, who also provided certain results in advance of publication. This research was supported in part by a NASA grant.

REFERENCES

Bhattacharyya, J. C., and Bappu, M. K. V. (1977). Nature **270**, 503.
Bouchet, P., Perrier, C., and Sicardy, B. (1980). IAU Circ. No. 3503.
Dunham, D. W. (1971). Ph.D. thesis, Yale University.
Elliot, J. L., Dunham, E., and Mink, D. (1977). Nature **267**, 328.
Elliot, J. L., Dunham, E., Wasserman, L. H., Millis, R. L., and Churms, J. (1978). Astron. J. **83**, 980.
Elliot, J. L., French, R. G., Frogel, J. A., Elias, J. H., Mink, D., and Liller, W. (1981a). Astron. J. **86**, 444.
Elliot, J. L., Frogel, J. A., Elias, J. H., Glass, I. S., French, R. G., Mink, D. J., and Liller, W. (1981b). Astron. J. **86**, 127.
Goldreich, P., and Tremaine, S. (1979a). Nature **277**, 97.
Goldreich, P., and Tremaine, S. (1979b). Astron. J. **84**, 1638.
Goldreich, P., and Tremaine, S. (1981). Astrophys. J. **243**, 1062.
Hubbard, W. B., and Zellner, B. H. (1980). Astron. J. **85**, 1663.
Klemola, A. R., and Marsden, B. G. (1977). Astron. J. **82**, 849.
Millis, R. L., and Wasserman, L. H. (1978). Astron. J. **83**, 993.
Millis, R. L.,Wasserman, L. H., and Birch, P. V. (1977). Nature **267**, 330.
Nicholson, P. D., Matthews, K., and Goldreich, P. (1981). Astron. J. **86**, 596.
Nicholson, P. D., Persson, S. E., Matthews, K., Goldreich, P., and Neugebauer, G. (1978). Astron. J. **83**, 1240.